Journal of Photochemistry & Photobiology, B: Biology 177 (2017) 76–84

Contents lists available at ScienceDirect

Journal of Photochemistry & Photobiology, B: Biology

journal homepage: www.elsevier.com/locate/jphotobiol

Photodynamic damage predominates on different targets depending on cell growth phase of *Candida albicans*

Alessandra Baptista[a,b], Caetano P. Sabino[a,c], Silvia C. Núñez[b], Walter Miyakawa[d], Airton A. Martin[b], Martha S. Ribeiro[a,*]

[a] Center for Lasers and Applications, Nuclear and Energy Research Institute, IPEN – CNEN/SP, São Paulo, SP, Brazil
[b] Biomedical Engineering Post-Graduation Program, Universidade Brasil, São Paulo, SP, Brazil
[c] Department of Microbiology, Institute for Biomedical Sciences, University of São Paulo, São Paulo, SP, Brazil
[d] Photonics Division, Institute for Advanced Studies, São José dos Campos, SP, Brazil

ARTICLE INFO

Keywords:
Adhesiveness
Atomic force spectroscopy
FT-IR spectroscopy
Stiffness
Ultrastructural study

ABSTRACT

Photodynamic inactivation (PDI) has been reported to be effective to eradicate a wide variety of pathogens, including antimicrobial-resistant microorganisms. The aim of this study was to identify the potential molecular targets of PDI depending on growth phase of *Candida albicans*. Fungal cells in lag (6 h) and stationary (48 h) phases were submitted to PDI mediated by methylene blue (MB) combined with a (662 ± 21) nm-LED, at 360 mW of optical power. Pre-irradiation time was 10 min and exposure times were 12 min, 15 min and 18 min delivering radiant exposures of 129.6 J/cm^2, 162 J/cm^2 and 194.4 J/cm^2, respectively, on a 24-well plate of about 2 cm^2 at an irradiance of 180 mW/cm^2. Scanning electron microscopy (SEM), transmission electron microscopy (TEM), atomic force spectroscopy (AFS) and Fourier transform infrared spectroscopy (FT-IR) were employed to evaluate the photodynamic effect in young and old fungal cells following 15 min of irradiation. Morphological analysis revealed wrinkled and shrunk fungal cell membrane for both growth phases while extracellular polymeric substance (EPS) removal was only observed for old fungal cells. Damaged intracellular structures were more pronounced in young fungal cells. The surface nanostiffness of young fungal cells decreased after PDI but increased for old fungal cells. Cellular adhesion force was reduced for both growth phases. Fungal cells in lag phase predominantly showed degradation of nucleic acids and proteins, while fungal cells in stationary phase showed more pronounced degradation of polysaccharides and lipids. Taken together, our results indicate different molecular targets for fungal cells in lag and stationary growth phase following PDI.

1. Introduction

Antimicrobial resistance is now recognized as one of the most serious global threats to human health in the 21st century [1]. In response, several research groups are in pursuit of alternative antimicrobial modalities. Antimicrobial photodynamic therapy or photodynamic inactivation (PDI) represents a therapeutic modality that involves the combination of a photosensitizer (PS) with light of appropriate wavelength and molecular oxygen to produce reactive oxygen species (ROS) that can inactivate microorganisms by oxidative stress. PDI itself is improbable to cause microbial resistance since damage by ROS is supposed to be through a nonspecific killing mechanism [2,3]. Reports in literature have confirmed its efficacy against pathogenic yeast, parasites, viruses, algae and bacteria [4,5,6]. In fact, depending on parameters PDI is capable to surpass the antioxidant defenses of cells and initiate a process of cellular death via different pathways [7].

Although PDI mechanisms seem to be very straightforward and, in theory, it can affect and destroy all cellular types, literature reports contradictory results [3,8]. In fact, PDI parameters such as light dosimetry [9], type and concentration of the photosensitizer [10] and environmental conditions (e.g. oxygen supply) [11] can influence its outcome. In addition, microbial defenses against ROS play a pivotal role in PDI susceptibility [12].

Microorganisms present many variances in different levels as cellular morphology, metabolism and adaptation to environmental conditions, i. e., cells young or old when living in the community have to deal with catabolites on the environment that promote different molecular signaling and according to that they will change their genic expression in order to survive affecting PDI results [3,13,14]. A microorganism growth curve is basically represented by five phases [15] in which microbial cells present distinct characteristics that influence PDI effectiveness [16]. In general, microbial cells in the log phase are

* Corresponding author at: Av. Lineu Prestes 2242, Cidade Universitária, 05508-000 São Paulo, SP, Brazil.
E-mail address: marthasr@usp.br (M.S. Ribeiro).

http://dx.doi.org/10.1016/j.jphotobiol.2017.10.013
Received 20 April 2017; Received in revised form 6 September 2017; Accepted 9 October 2017
Available online 10 October 2017
1011-1344/

more susceptible to PDI compared to other phases [16], however the mechanisms behind microorganism survival to PDI concerning growth phase have not been fully established. In addition, microorganisms tend to form surface-attached biofilm in different environments. Biofilms consist of microbial cells in different growth phases and a wide-ranging of self-generated extracellular polymeric substances (EPS), including polysaccharides, nucleic acids, and proteins [17].

In this study, we cultured *Candida albicans* cells in lag and stationary phases and used three radiant exposures to verify cell killing after methylene blue-mediated PDI. We designed experiments using young (6 h) and old (48 h) fungal cells to identify molecular targets that could improve PDI outcome. Thus, we used scanning electron microscopy (SEM) and transmission electron microscopy (TEM) to visualize morphological and ultrastructural variations following PDI as well as to analyze cellular nanomechanical and biochemical characteristics through atomic force spectroscopy (AFS) and Fourier transform infrared spectroscopy (FT-IR), respectively. *C. albicans* is a suitable model to link PDI tolerance to different growth phases due to its complexity that includes dimorphism as well as ability to resist to antifungals [18,19] and oxidative stress [19,20].

2. Material and Methods

2.1. Yeast Strains and Inocula

Candida albicans suspensions (ATCC 90028) were cultured from vial stocks onto Sabouraud broth dextrose under aerobic conditions at 37 °C in an orbital shaker (100 rpm). Yeast inocula were taken from 6 h (lag phase) and 48 h (stationary phase) growth stage. After that, cells were washed, suspended in phosphate-buffered saline (PBS), and turbidity of cell suspensions was measured in an optical spectrophotometer (Spectramax M4, Molecular Devices, Sunnyvale, Ca, USA) to obtain suspensions of 1×10^7 cells/mL (optical density of 1.0 at $\lambda = 540$ nm).

2.2. Photosensitizer/Light Source and Irradiation Conditions

A stock solution of 5 mM of commercially available methylene blue (MB) (dye content ≥ 82%, Sigma-Aldrich, MO, USA) was prepared in distilled water without further purification. The MB solution was filtered through a sterile 0.22 μm membrane and stored in the dark. For experiments, MB was added to the yeast suspension to give a final working concentration of 50 μM [12].

The light source used for the MB excitation was a custom-made single light emitting diode (LED) with peak emission at $\lambda = 662 \pm 21$ nm and optical power of 360 mW. The LED tip was fixed on a holder that kept the beam area at about 2 cm^2, which coincided to the single well area from the 24-well microtiter plate (Fig. 1). The pre-irradiation time was set as 10 min. Aliquots were illuminated with irradiance of 180 mW/cm^2 for 12 min, 15 min and 18 min, delivering radiant exposures of 129.6 J/cm^2, 162 J/cm^2 and 194.4 J/cm^2, respectively.

2.3. Antimicrobial Photodynamic Therapy

C. albicans suspensions were placed in wells of a 24-well microtiter plate and irradiated individually from top to bottom. The samples were divided into six groups as shown in Table 1. For all groups, the experiments were performed with 990 μL of *C. albicans* suspension adding either 10 μL of sterile distilled water (control and LED groups) or 10 μL of MB aqueous solution (control PS and experimental groups). Assays were performed in triplicate at three different days corresponding to n = 9/group.

2.4. Microbiological Analysis

C. albicans suspensions were serially diluted in PBS to give dilutions of 10^{-1} to 10^{-5} times the original concentration. Ten-μL aliquots of each dilution were streaked vertically onto Sabouraud agar plates in triplicate and incubated at 37 °C overnight [21]. On the following day, yeast colonies were counted and converted into CFU/mL. The survival fraction values were calculated by dividing the obtained data by the mean of control group.

The next assays were performed using only one exposure time determined from the microbiological results.

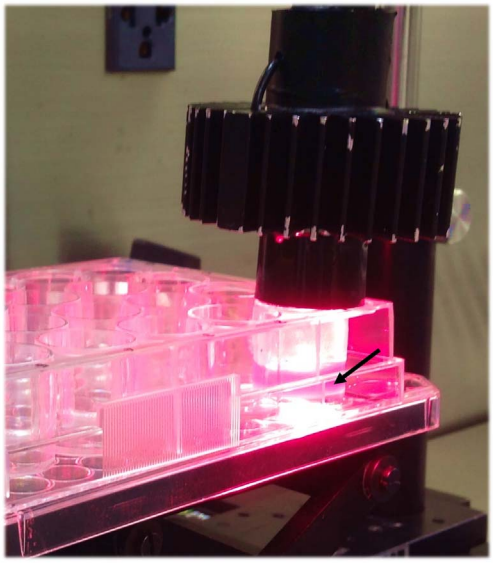

Fig. 1. Illustrative image of experimental setup. Notice the LED tip covering the single well area of the 24-well microtiter plate (2 cm^2). The arrow points to the MB-stained *C. albicans* suspension.

Table 1
Experimental groups.

Groups	LED	MB
Control group (L_-/MB_-)	−	−
LED Group, (L_+/MB_-) (18 min)	+	−
MB Group 50 μM (L_-/MB_+)	−	+
PDI, 12 min	+	+
PDI, 15 min	++	+
PDI, 18 min	+++	+

2.5. Scanning Electron Microscopy (SEM)

Fungal cell suspensions from lag and stationary phases of control and PDI groups were diluted in distilled water and fixed in 2% glutaraldehyde for 2 h. Next, samples were washed three times in distilled water and incubated in 10 mM $Ru(bipy)_3$ (Sigma-Aldrich, MO, USA) during 30 min. Specimens were washed again and the supernatants removed. The suspensions were then deposited on glass coverslips and air-dried at room temperature. Thereafter, the samples were placed on a metallic holder and analyzed by a scanning electron microscope (TM 3000 Tabletop, Hitachi, Tokyo, Japan).

2.6. Transmission Electron Microscopy (TEM)

Nontreated and PDI suspension samples of *C. albicans* (6 h and 48 h) were fixed in 2% glutaraldehyde overnight, at 4 °C. Samples were then centrifuged at 1200 rpm, 10 min and fixative solution was replaced by 0.1 M sodium cacodylate buffer (pH 7.2). The cell pellets were postfixed in 2% OsO_4 in sodium cacodylate buffer, dehydrated in a graded alcohol series, and embedded in low viscosity Spurr resin (Tousimis, Rockville, MD). Ultrathin sections were cut on a ultra-microtome

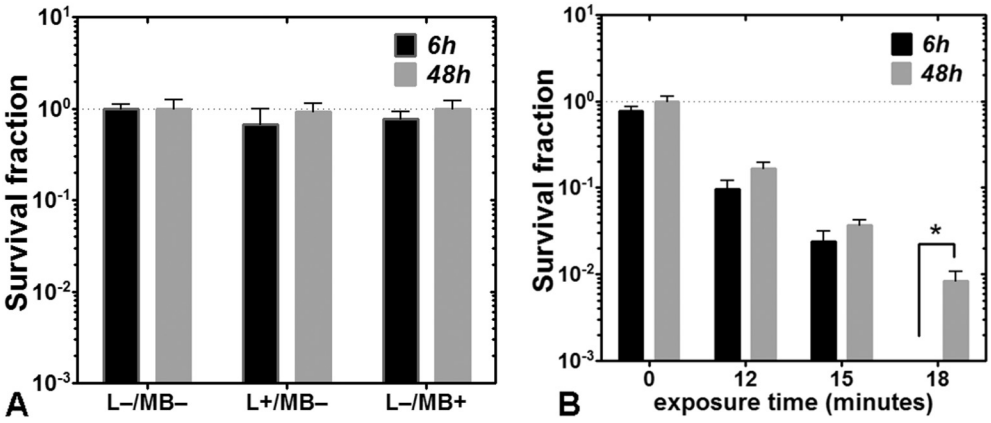

Fig. 2. Effects of PDI on *C. albicans* cells in different growth phases. A: Control (L_-/MB_-, LED (L_+/MB_-) and MB (L_-/MB_+) groups; B: Three different radiant exposures were evaluated (12 min, 15 min and 18 min). The symbol * represents a statistically significant difference after 18 min of irradiation ($p < 0.05$). Data represent mean values and bars are standard deviations.

(Leica, Germany), collected on uncoated 200-mesh copper grids, stained with uranyl acetate and lead citrate, and examined on a transmission electron microscope (JEOL, model 1010, Tokyo, Japan) using an accelerating voltage of 80 kV.

2.7. Atomic Force Spectroscopy (AFS)

Suspensions of *C. albicans* in lag and stationary phases from control and PDI groups were washed out by centrifugation for 3 min at 2400 rpm, had the supernatant removed and resuspended in 1 mL of sterile distilled water, for three times. After the third discard of supernatant, 10 μL aliquots of the pellets were spread over a clean glass coverslip and air-dried at room temperature [22].

The SPM-9500 J3 atomic force microscope (Shimadzu Corporation, Japan) microscope operated in contact mode to image the cells and obtain force-distance curves. Silicon nitride (Si_3N_4) cantilevers, with ~20 nm tip nominal radius of curvature were used. The cantilever deflection was calibrated with an AISI 304 stainless steel sample. Ten force curves were obtained for each group sample in three different days, resulting n = 30.

The SPM-9500 series software (2.40 version) was operated to analyze images and force curves. For force-distance curve evaluation, cantilever tips with ~0.10 N/m elastic constant were used. The force-distance curve represents the tip-sample interaction forces X z piezo position. Nanomechanical properties such as surface stiffness can be calculated from the slope of the curve. The surface stiffness was estimated through the ratio between tip-sample force and piezo position [23].

The adhesion force was directly obtained from the minimum force at the point where the tip is released from the contact with the sample.

2.8. Fourier Transform Infrared Spectroscopy (FT-IR)

Suspensions of *C. albicans* before and after PDI (6 h and 48 h) were washed 3 times by centrifugation for 3 min at 2400 rpm followed by resuspension of pellets in 1 mL of sterile distilled water. Supernatants were removed and the remaining pellets were suspended in 100 μL of sterile distilled water, vortexed for 40 s to obtain a homogeneous cell suspension, and aliquots (5 μL) were deposited on CaF_2 windows previously washed with detergent and water, disinfected with 70% ethanol and dried with paper towels.

For each sample, we obtained 10 spectra ranging from 4000 cm^{-1} to 900 cm^{-1} with 2 cm^{-1} spectral resolution using a Spectrum Spotlight 400 FT-IR spectrophotometer (Perkin Elmer Walthan, MA, USA). The background spectrum was taken at a clean cell-free place on the CaF_2 window at each change of reading.

Spectra were analyzed using the OPUS spectroscopy software (version 4.2, Bruker). Spectral curves were subjected to baseline correction (Rubberband correction, 32 points and CO_2 bands subtraction) and the mean spectrum was obtained using the statistical feature of the OPUS.

The whole spectrum was divided into four spectral windows according to main cellular biochemical components [24]. The range between 3000 and 2800 cm^{-1}, which is influenced by functional groups of membrane fatty acids; the range between 1800 and 1500 cm^{-1}, relative to amide I and amide II groups belonging to proteins and peptides; the range between 1500 and 1200 cm^{-1}, mixed region influenced by proteins, fatty acids and phosphate-carrying compounds; the range between 1200 and 900 cm^{-1}, which is informative mostly for the carbohydrates and polysaccharides in the cell wall.

2.9. Statistical Analysis

Shapiro-Wilk test was applied to check normality of data distribution. Data were compared using one-way ANOVA and Tukey as a post-hoc test. Statistically significant differences were considered when $p < 0.05$.

3. Results and Discussion

The microbiological analysis showed that the mean values of CFU/mL (± standard error) of *C. albicans* control cells or light treated did not present statistically significant reduction ($p > 0.05$) as well as a 50 μM concentration of MB did not show any toxicity for yeast cells after incubation for 10 min in the dark for the two growth phases ($p > 0.05$) Fig. 2A). After 12 min and 15 min of irradiation, comparable reduction in cell viability was observed in lag and stationary growth phases. However, after 18 min of irradiation we noticed a complete eradication in number of viable young cells (6 h) of *C. albicans*, while old cells reduced only 2 logs (48 h) (Fig. 2B).

Our results corroborate the literature since the efficiency of microorganism photoinactivation is intimately related to its physiological state [16]. This result is probably due to the protection acquired by old cells against oxidative stress [19]. Although lag phase is a poorly understood growth phase, it has been assumed that this phase allows the adaptation required by the cells to begin to exploit new conditions, developing some resistance against environmental threatening including ROS [25].

Interestingly, microbiological analysis showed that 6 h and 48 h-cells exhibited similar behavior after PDI at the lowest radiant exposures. Thus, we proceeded with experiments using *C. albicans* in lag and stationary phases exposed to 15 min of PDI expecting to obtain some leads to the possible targets of ROS.

SEM images of control groups showed highly dense and compacted cells exhibiting smooth surfaces (Fig. 3). Cells in lag phase revealed spherical form and the presence of hyphal filament (Fig. 3A and B), while cells in stationary phase also showed round shape covered with EPS (Fig. 3E and F).

Following PDI, cells of both groups shrunk and displayed a wrinkled

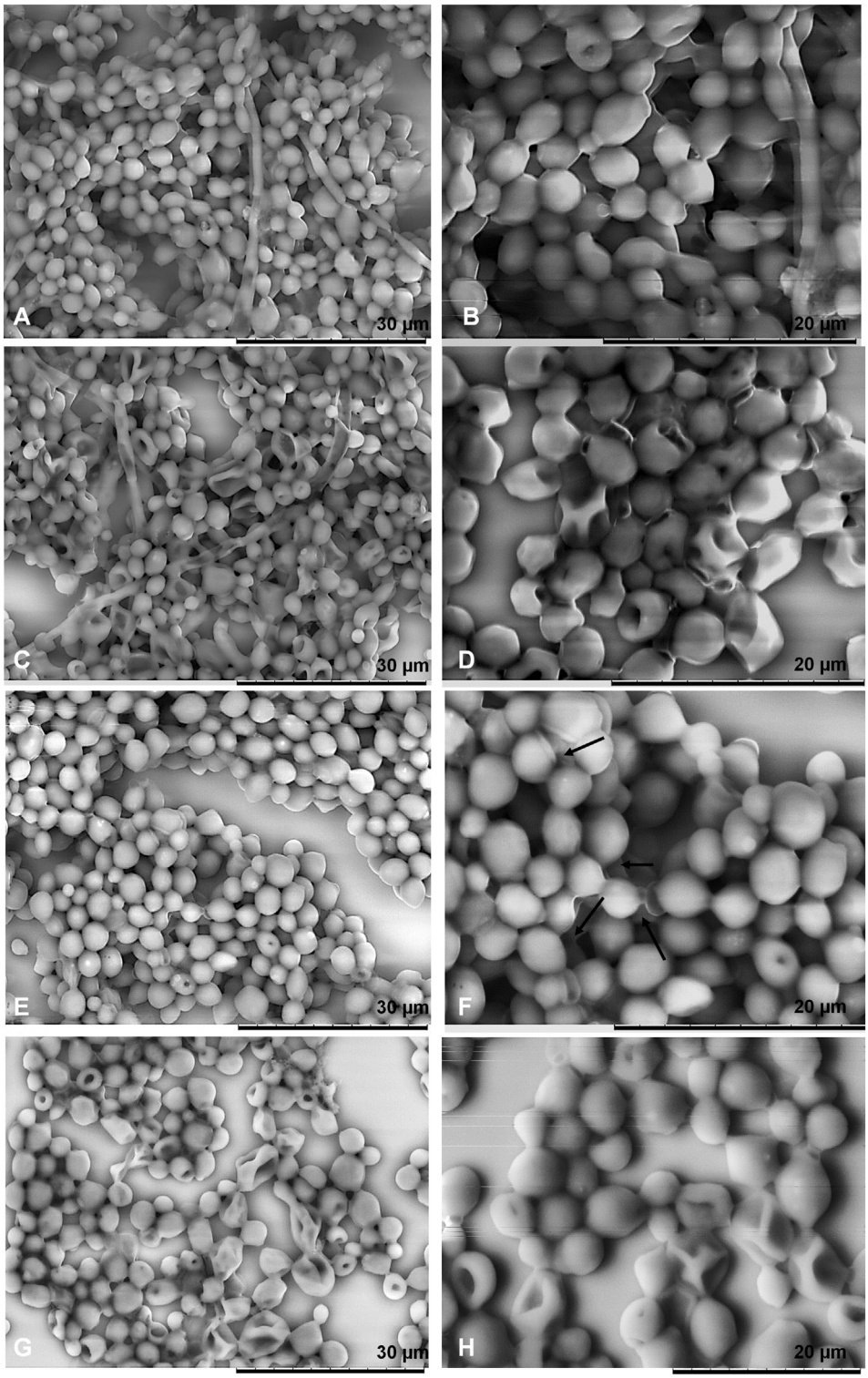

Fig. 3. Electron-micrographs of *C. albicans* cells observed by SEM. A and B: 6 h-cells of control group; C and D: 6 h-cells following PDI 15 min; E and F: 48 h-cells of control group; G and H: 48 h-cells following PDI 15 min. Black arrows point to the presence of EPS. Scale bars represent 30 µm (A, C, E, G) and 20 µm (B, D, F, H).

superficial appearance (Fig. 3D to H). In addition, we observed the removal of EPS after PDI in cells grown for 48 h (Fig. 3G and H). Literature has demonstrated that EPS is the first target affected by PDI mainly using cationic photosensitizers [17,26]. As the EPS is also composed by proteins, it is expected that they quench singlet oxygen and, therefore, the fungal reduction could be not effective [27]. Furthermore, EPS acts as a physical barrier preventing PS diffusion into cells, which would allow damage on vital organelles [28,29].

Fig. 4 shows TEM images of untreated and exposed to 15 min cells of *C. albicans* cultured by 6 h and 48 h. For both growth phases, control cells exhibited a regular outlined cell wall, cell membrane integrity, cell organelles with prominent nucleus, vacuoles and some dense bodies regularly distributed over the cytoplasm (Fig. 4A–B and 4E–F). It is also possible to notice that old cells present thicker cell wall than young cells. In fact, it has been reported that the cell wall in the stationary phase is thicker and less permeable to macromolecules than those in the exponential phase [30,31]. Changes in the cell wall occur depending on the phase of the cell cycle, nutrient availability, and environmental conditions such as pH, temperature, and availability of oxygen [31]. Significant changes that occur in the medium during stationary phase,

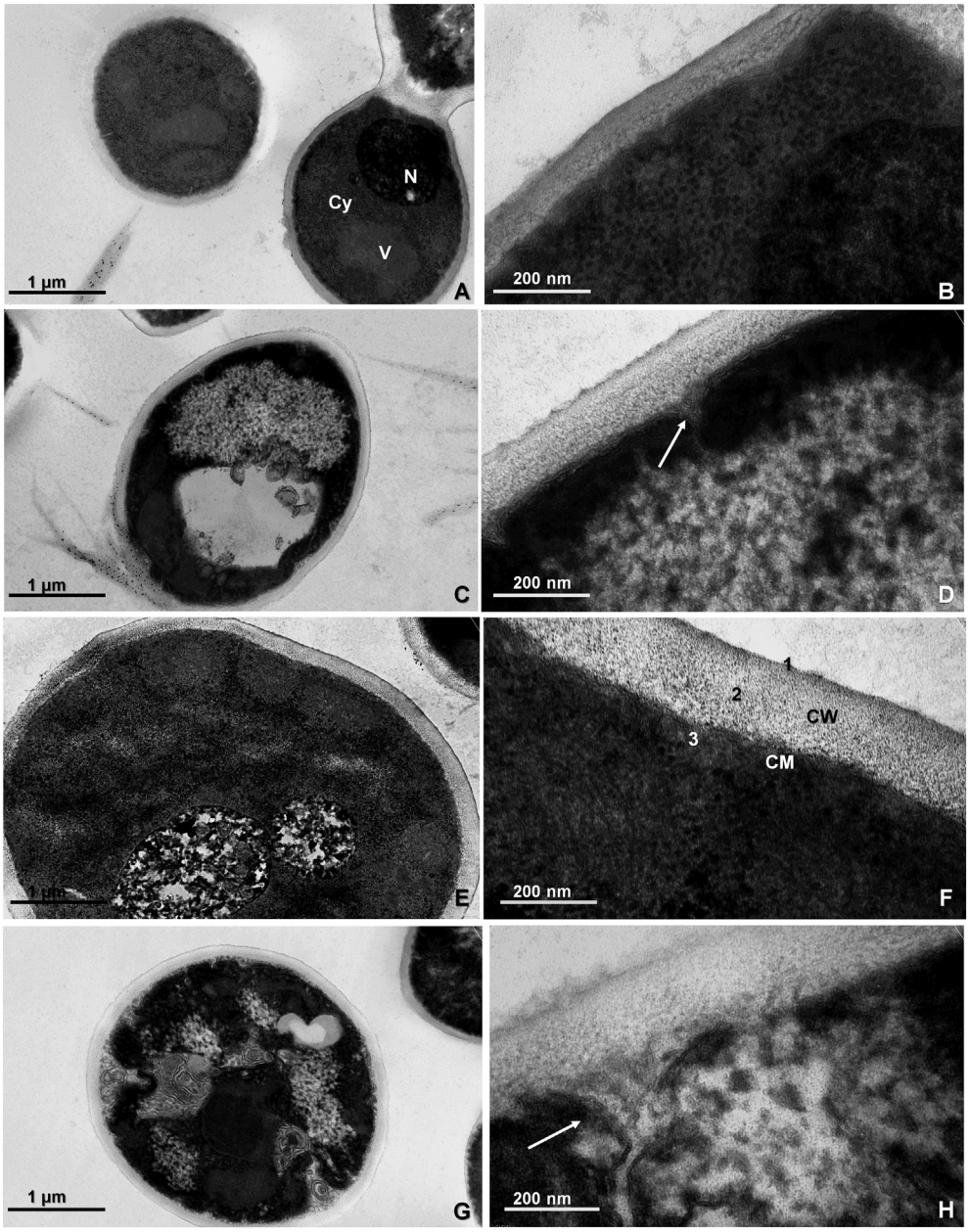

Fig. 4. Electron-micrographs of *C. albicans* cells observed by TEM. (A and B: 6 h-cells of control group; C and D: 6 h-cells following PDI 15 min; E and F: 48 h-cells of control group; G and H: 48 h-cells following PDI 15 min. (1) outer mannoproteins fibrillar layer; [2] inner cell wall layers with predominance of glucans and chitin; [3] cell membrane. White arrows indicate cell membrane damage. N: nucleus; V: vacuole; Cy: cytoplasm. Scale bars represent 1 µm (A, C, E, G) and 200 nm (B, D, F, H).

as the depletion of available nutrients and pH decrease [32], lead to stress adaptation [33] and, consequently, cell wall thickening.

After PDI, 6 h and 48 h-cells displayed notable differences in the cell wall, cell membrane and cytoplasm. Cell membrane and internal structures were more affected in young cells, while old cells showed loose fibrillar and inner cell wall layers besides loss of cell membrane integrity (Fig. 4C–D and G–H).

The literature reports that cell wall plays an important role in the response to oxidative stress [34], once the cell wall is essential to maintain the cell integrity, and any severe damage in its morphology can cause alterations in its function [35]. If morphological and ultrastructural changes are involved in the mechanisms of adaptation to oxidative stress, the AFS can be a useful complementary technique to evaluate stiffness and adhesiveness of the cell wall.

Before PDI, young cells showed higher stiffness compared to old cells ($p < 0.05$) (Fig. 5A). After PDI, 6 h-cells decreased rigidity, while 48 h-cells were more rigid ($p < 0.05$) (Fig. 5A). Conversely, the adhesion force of young cells was lower compared to old cells ($p < 0.05$). However, after PDI both 6 h and 48 h-cells diminished adhesiveness ($p < 0.05$) (Fig. 5B).

The fungal cell wall consists of polymers that are interconnected to produce a complex structure composed of an inner layer of a β-1,3-glucan branched with chitin, that are responsible for mechanical strength of cell wall, and an outer layer of a β-1,6-linked glucans branched on the β-1,3-glucan network, also linked to the mannoproteins [36]. The elasticity of the cell wall could be attributed to the β-1,3-glucan fibrillar network [37]. Cell wall construction is mainly coordinated with progress of the cell cycle. During lag phase, and not during any other phase of the cell cycle, produced chitin is laid down in the lateral walls stabilizing the wall of the future mother cell [37]. Studies show that chitin plays an important role in the elasticity of the cell wall [38,39]. The difference in nanomechanical properties of the cell walls at distinct growth phases are probably connected with its molecular architecture, even though the cell wall composition is seemingly comparable [40].

The cell wall is a dynamic structure and undergoes remodeling in response to oxidative stress [41]. The ROS generated react with structures such as polysaccharides, proteins, lipids and nucleic acids

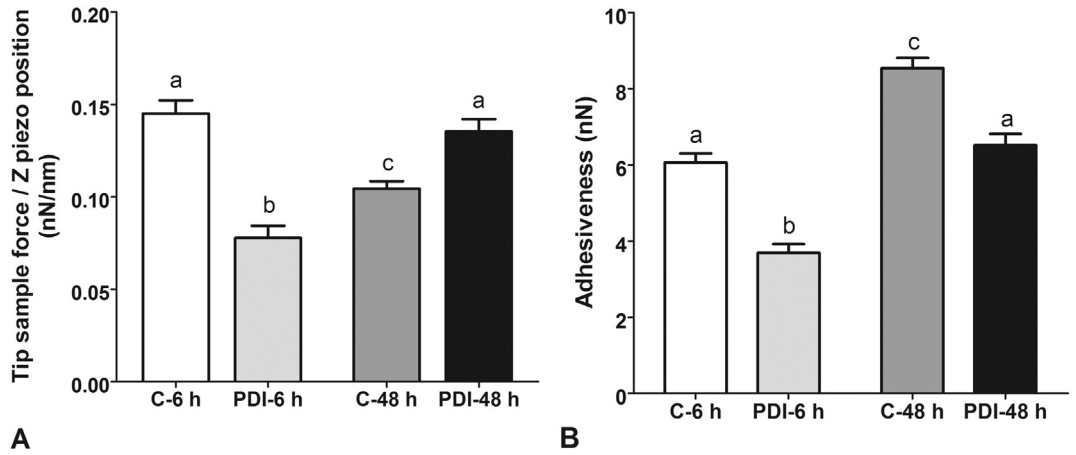

Fig. 5. Comparison of stiffness (A) and adhesiveness (B) of *C. albicans* cells in lag (6 h) and stationary (48 h) phases. PDI group is related to 15 min of exposure time. The data represent the mean values of untreated and treated cells. Bars are standard errors. Different letters denote statistically significant differences among groups ($p < 0.05$).

Table 2
Assignment of peak frequencies obtained for untreated and submitted to PDI young and old cells.

Range spectral	Frequency (cm^{-1})	Assignment
1200–900	911	Mannans
C—O—C, C—O of ring vibrations of the carbohydrates	966	C—O ribose, C—C
	998	β(1 → 6) glucans
	1024	β(1 → 4) glucans
	1045	C—O stretching frequencies coupled with C—O bending frequencies of the C—OH groups of carbohydrates
	1060–1030	S═O
	1084–1088	P═O stretching of PO^{-}_2 phosphodiesters
	1080	β(1 → 3) glucans
	1106	β(1 → 3) glucans
	1117	C—O stretching vibration of C—OH group of ribose (RNA)
	1160	CO stretching
1800–1500	1205	C—O—C, C—O ring vibrations of polysaccharides
Amide II groups belonging to proteins and peptides	1245	PO^{-}_2 asymmetric (phosphate)
	1400	Symmetric stretching vibration of COO^{-} group of fatty acids and amino acids δ_s CH_3 of proteins; CH3 bending vibration (lipids and proteins)
	1550	Amide II of proteins
	1630	Amide I; α-quitin
	1650	Amide I; α-quitin
	1727	C═O stretching band mode of the fatty acid ester
2800–3100		C—H; lipid region; CH_3, CH_2 – lipid and protein; fatty acids
C—H stretching vibrations of methyl (CH3) & methylene (CH2) groups & olefins		

inducing molecular alterations that can negatively affect cellular physiology and morphology [42]. After PDI, the apparent lower stiffness in young cells is probably related with the association of membrane lipid oxidation and damage of internal structures such as the cytoskeleton. Hence, in the approach branch of the force spectroscopy, the tip would push the cell surface more easily. In fact, Schiavone and coworkers reported that cell wall stiffness is in part dependent on the integrity of the cell membrane [42].

On the other hand, old cells showed themselves less elastic after EPS was removed. The protective feature of the EPS in stationary cells suggests a natural compensatory defense to the lower softness of the membranes of older cells. Naturally, the cell membranes of young cells should be more rigid to compensate the lower amount of EPS. In old cells, the increased rigidity suggests a defense cell mechanism to the EPS reduction during PDI as the EPS is the first target of the ROS.

Remarkably, AFS measures show that old and young cells decrease adhesiveness following PDI. This finding fits with SEM images since cells appeared wrinkled and contracted disregarding the growth phase. Besides, EPS is removed following PDI, which reduces the adhesion force.

FT-IR spectral profiles were obtained from untreated and treated *C. albicans* in lag phase and stationary phase to identify potential molecular components in yeast cells that are predominant targets of photooxidation and correlate with data obtained through morphological, ultrastructural and nanomechanical analysis. Table 2 exhibits the peak frequencies that have been obtained from the second derivate spectra (data not shown). Strong absorption bands were detected in all spectral regions that characterize the major cellular constituents (1200–900 cm^{-1}; 1500–1200 cm^{-1}; 1800–1500 cm^{-1} and 3000–2800 cm^{-1}) (Figs. 6A–B, and 7A–D).

We also analyzed the spectra of difference to highlight the biochemical alterations between old and young cells of control group (Fig. 6C and D) and between control and PDI groups (Fig. 7E and F). The spectral difference between 6 h and 48 h-cells shows that cells in stationary phase presented a higher amount of polysaccharides compared to cells in lag phase (Fig. 6C and D). These data corroborate our previous results once fungal cells in the stationary phase show greater abundance of EPS than fungal cells in lag phase. In fact, it is well-known that EPS of *C. albicans* is composed mainly by polysaccharides [43,44]. On the other hand, young fungal cells displayed a higher amount of

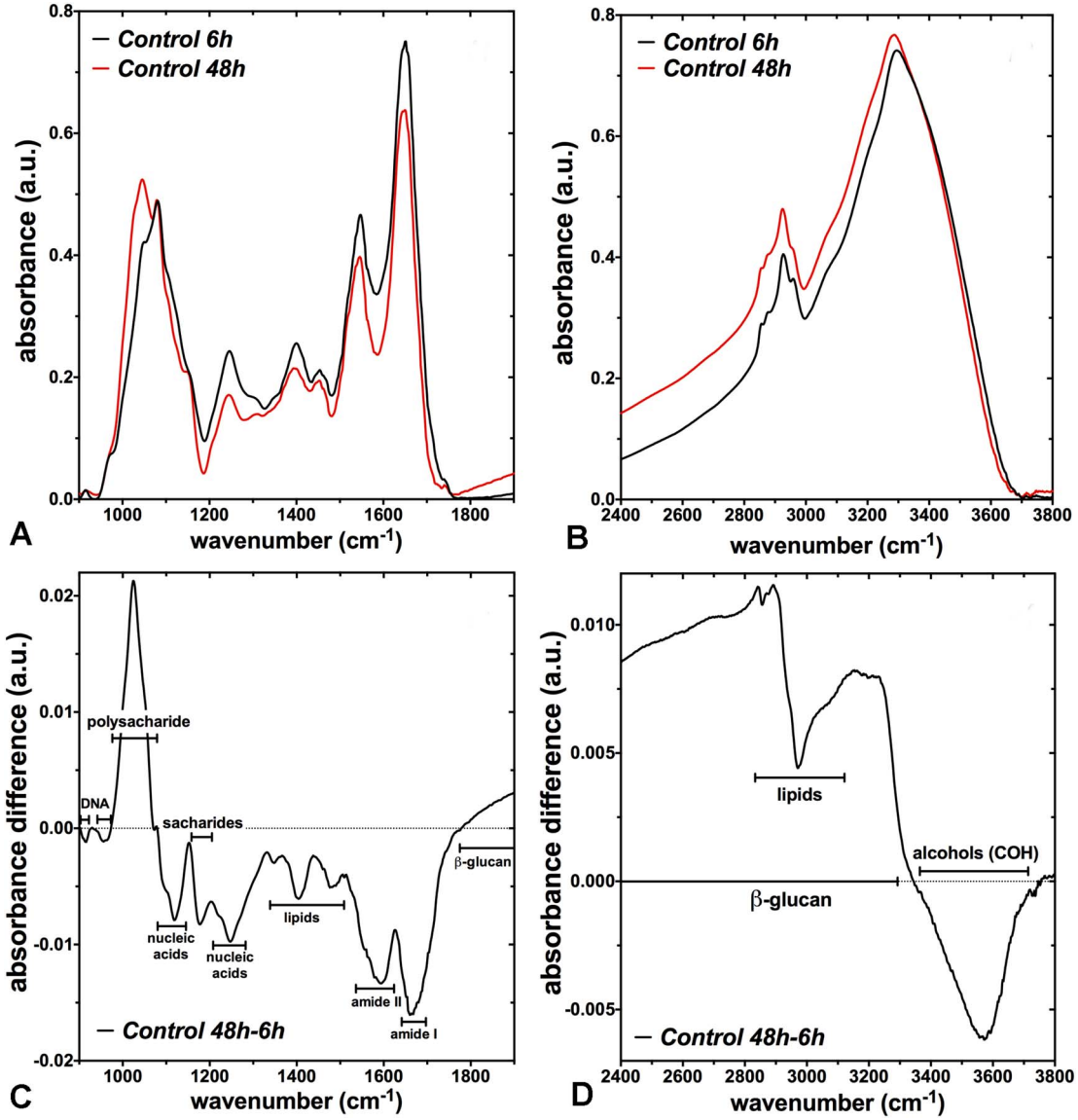

Fig. 6. A and B: Normalized FT-IR spectra of *C. albicans* control cells in lag (6 h) and stationary (48 h) phases. C and D: Spectral difference between old (48 h) and young (6 h) cells.

nucleic acids, lipids and proteins. This finding was also expected since lag phase fungal cells are adapting to enter the highly proliferative exponential phase by means of increased nucleic acid metabolism besides protein and fatty acid biosynthesis [25].

Fig. 7E and F exhibit the subtraction of the spectra presented in Fig. 7A to D. After PDI, we observed a dynamic pattern of formation and degradation of molecular functional groups above and below the zero line, respectively. These findings are in agreement with other authors, since when a cell damage by oxidative stress can occur in cell wall and cause lipidic peroxidation, protein carbonylation and antioxidant synthesis [34,41]. *C. albicans* cells in lag phase showed degradation of functional groups related to C—O of deoxyribose, C—C of DNA; C—O stretching vibration of C—OH group of ribose-RNA; P—O stretching modes originated from the phosphodiester groups of nucleic acids; C═C, C═N, C═O, N═H of proteins and amides (internal damage). On the other hand, cells in stationary phase showed further decreases of C—O groups of polysaccharides, β-glucans, and lipids, suggesting high levels of cell wall and cell membrane damage.

Taken together, our results suggest that depending on the growth phase, PDI acts on different structures. In fact, localization of the photosensitizer plays a pivotal role to determine the possible targets in PDI.

The MB used in this study was a commercially available dye that was employed without further purification. It is known upon irradiation MB suffers degradation and the demethylation of the amino residues leads to the formation of Azure stains and other products [45]. Different photosensitizers (e.g., phenotiazines, porphyrins, triarylmethanes) may alter the affinity of the dye to distinct biological targets [46,47] and new studies should be performed towards the binding approach of photoantimicrobials to cell targets in order to improve PDI.

Uptake of exogenous substances by yeast cells is adversely affected by lipophilicity and positively affected by hydrophilicity besides the presence of charged groups [48]. Thus, cells in stationary phase, which are more abundant in polysaccharides are able to retain MB and EPS within cell wall have the greatest probability of being involved in photodynamic processes [48]. Contrarily, this barrier for young cells is not pronounced allowing the diffusion of photosensitizer across the membrane, promoting the destruction of organelles and other intracellular structures.

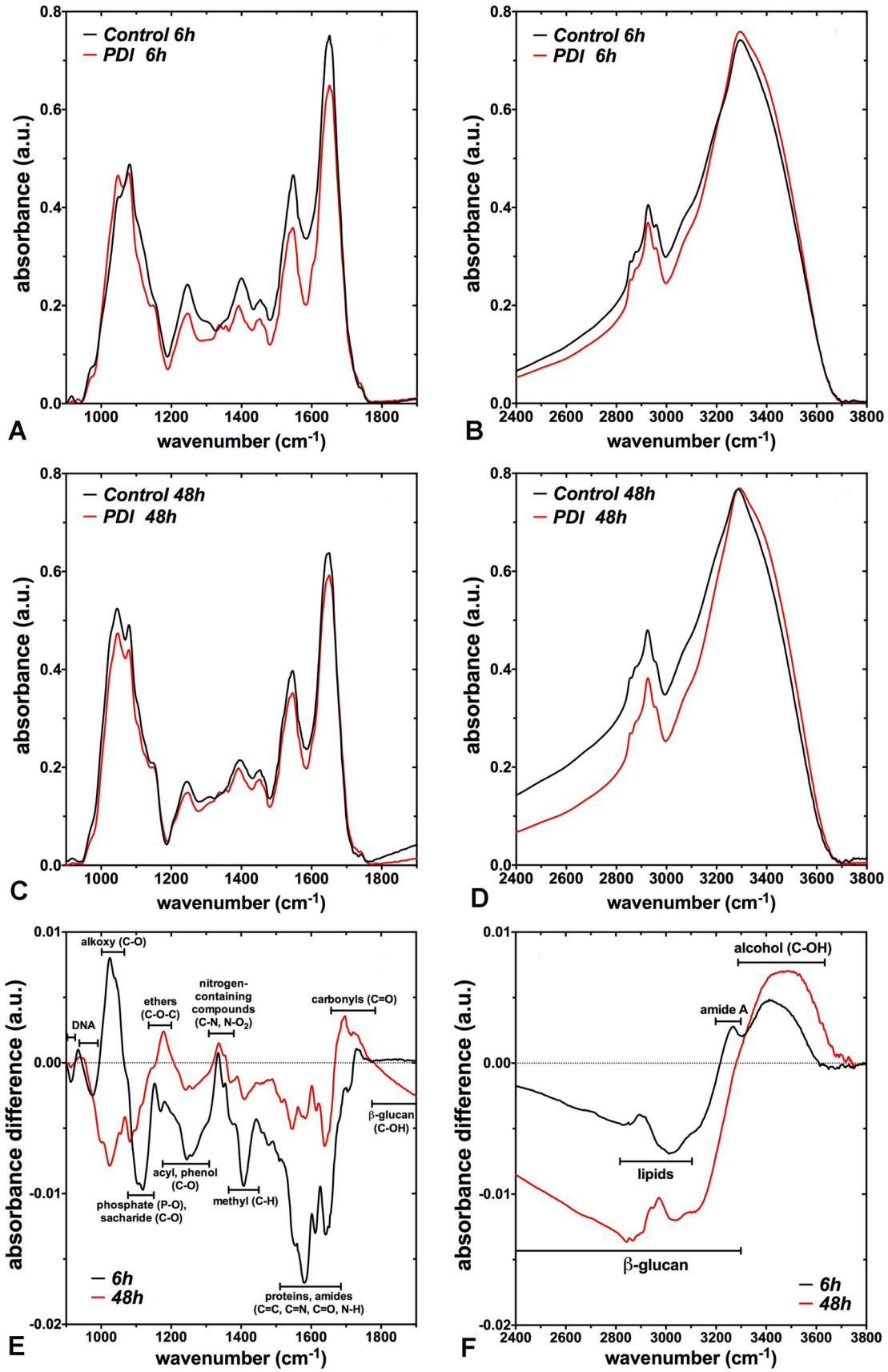

Fig. 7. A and B: Normalized FT-IR spectra of untreated and treated *C. albicans* cells in lag phase (6 h); C and D: Normalized FT-IR spectra of untreated and treated *C. albicans* cells in stationary phase (48 h); E and F: Spectral difference between control and PDI 15 min groups for young (6 h) and old (48 h) cells.

4. Conclusion

For the first time it was identified different targets for MB-mediated PDI depending on growth phase of *Candida albicans* cells by SEM, TEM, AFS and FT-IR spectroscopy. Young fungal cells showed greater internal damage while in old fungal cells, the EPS, cell wall and membrane appeared to be the first target. Other types of fungal and bacterial cells as well as different photosensitizers should be tested to improve PDI outcome. We expected that this work encourages new researches in pursuing better understanding in PDI biological mechanisms.

Acknowledgements

The authors thank FAPESP (grant #10/13313-9) and CNPQ (grant INCT-573916/2008) for financial support and the Centro de Ciência e Tecnologia de Plasmas e Materiais - PlasMat, Institute of Aeronautics Technology, for the AFM facility. Authors are also acknowledged to Thiago M. Pereira and Tania M. Yoshimura for helpful discussion.

References

[1] WHO, WHO Library Cataloguing-in-Publication Data, 1 World Health Organization, Geneva, 2014 232.
[2] T. Maisch, Resistance in antimicrobial photodynamic inactivation of bacteria, Photochem. Photobiol. Sci. 14 (8) (2015).
[3] M.H. Hamblin, Antimicrobial photodynamic inactivation: a bright new technique to kill resistant microbes, Curr. Opin. Microbiol. 33 (2016) 67–73.
[4] L.M. Baltazar, A. Ray, D.A. Santos, P.S. Cisalpino, A.J. Friedman, J.D. Nosanchuk, Antimicrobial photodynamic therapy: an effective alternative approach to control fungal infections, Front. Microbiol. 13 (6) (2015) 202.
[5] J.G. Pinto, L.C. Fontana, M.A. de Oliveira, C. Kurachi, L.J. Raniero, J. Ferreira-Strixino, In vitro evaluation of photodynamic therapy using curcuminute on *Leishmania major* and *Leishmania braziliensis*, Lasers Med. Sci. 31 (5) (2016) 883–890.
[6] F.P. Sellera, C.P. Sabino, M.S. Ribeiro, R.G. Gargano, N.R. Benites, P.A. Melville, F.C. Pogliani, In vitro photoinactivation of bovine mastitis related pathogens, Photodiagn. Photodyn. Ther. 13 (2016) 276–281.
[7] F. Vatansever, W.C. de Melo, P. Avci, D. Vecchio, M. Sadasivam, A. Gupta, R. Chandran, M. Karimi, N.A. Parizotto, R. Yin, G.P. Tegos, M.R. Hamblin, Antimicrobial strategies centered around reactive oxygen species—bactericidal antibiotics, photodynamic therapy, and beyond, FEMS Microbiol. Rev. 37 (6) (2013) 955–989.
[8] F. Javed, L.P. Samaranayake, G.E. Romanos, Treatment of oral fungal infections using antimicrobial photodynamic therapy: a systematic review of currently available evidence, Photochem. Photobiol. Sci. 13 (5) (2014) 726–734.
[9] R.A. Prates, E. da Silva, A.M. Yamada, L.C. Suzuki, C.R. Paula, M.S. Ribeiro, Light parameters influence cell viability in antifungal photodynamic therapy in a fluence and rate fluence-dependent manner, Laser Phys. 19 (5) (2009) 1038–1044.
[10] S.F. Vilela, J.C. Junqueira, J.O. Barbosa, M. Majewski, E. Munin, A.O. Jorge, Photodynamic inactivation of *Staphylococcus aureus* and *Escherichia coli* biofilms by malachite green and phenothiazine dyes: an in vitro study, Arch. Oral Biol. 57 (6) (2012) 704–710.
[11] D.E. Dolmans, D. Fukumura, R.K. Jain, Photodynamic therapy for cancer, Nat. Rev. Cancer 3 (2003) 380–387.
[12] I.T. Kato, I.T. Kato, R.A. Prates, C.P. Sabino, B.B. Fuchs, G.P. Tegos, E. Mylonakis, M.R. Hamblin, M.S. Ribeiro, Antimicrobial photodynamic inactivation inhibits *Candida albicans* virulence factors and reduces in vivo pathogenicity, Antimicrob. Agents Chemother. 57 (1) (2013) 445–451.
[13] G. Jori, C. Fabris, M. Soncin, S. Ferro, O. Coppellotti, D. Dei, L. Fantetti, G. Chiti, G. Roncucci, Photodynamic therapy in the treatment of microbial infections: basic principles and perspective applications, Lasers Surg. Med. 38 (5) (2006) 468–481.
[14] L. Yao, Q. Rong, A. Sebastian, J. Zaat, B. Eefjan, H. Michal, Antibacterial photodynamic therapy: overview of a promising approach to fight antibiotic-resistant bacterial infections, J Clin Transl Res 1 (3) (2015) 140–167.
[15] S.E. Finkel, Long-term survival during stationary phase: evolution and the GASP phenotype, Nat. Rev. Microbiol. 4 (2) (2006) 113–120.
[16] F. Gad, T. Zahra, T. Hasan, M.R. Hamblin, Effects of growth phase and extracellular slime on photodynamic inactivation of gram-positive pathogenic bacteria, Antimicrob. Agents Chemother. 48 (6) (2004) 2173–2178.
[17] W.C.M.A. de Melo, P. Avci, M.N. de Oliveira, A. Gupta, D. Vecchio, M. Sadasivam, R. Chandran, Y.-Y. Huang, R. Yin, L.R. Perussi, G.P. Tegos, J.R. Perussi, T. Dai, M.R. Hamblin, Photodynamic inactication of biofilm: talking a lightly colored approach to stubborn infection, Expert Rev. Anti-Infect. Ther. 11 (7) (2013) 669–693.
[18] R.A. Calderone, *Candida* and candidiasis, ASM Press, 2002.
[19] F.L. Mayer, D. Wilson, B. Hube, *Candida albicans* pathogenicity mechanisms, Virulence 4 (2) (2013) 119–128.
[20] M. Sanguinetti, B. Posteraro, C. Lass-Florl, Antifungal drug resistance among *Candida* species: mechanisms and clinical impact, Mycoses 58 (2) (2015) 2–13.
[21] B.D. Jett, K.L. Hatter, M.M. Huycke, M.S. Gilmore, Simplified agar plate method for quantifying viable bacteria, BioTechniques 23 (4) (1997) 648–650.
[22] A.V. Bolshakova, O.I. Kiselvova, A.S. Filonov, O.Y. Frolova, Y.L. Lyubchenklo, I.V. Yaminutesky, Comparative studies of bacteria with an atomic force microscopy operating in different modes, Ultramicroscopy 86 (1–2) (2001) 121–128.
[23] Y. Hashimoto, A. Nishiura, N. Matsumoto, Atomic force microscopy observation of enamel surfaces treated with self-etching primer, Dent. Mater. J. 32 (1) (2013) 181–188.
[24] D. Naumann, D. Helm, H. Labischinski, Microbiological characterizations by FT-IR spectroscopy, Nature 351 (6321) (1991) 81–82.
[25] M.D. Rolfe, C.J. Rice, S. Lucchini, C. Pin, A. Thompson, A.D. Cameron, M. Alston, M.F. Stringer, R.P. Betts, J. Baranyi, M.W. Peck, J.C. Hinton, Lag phase is a distinct growth phase that prepares bacteria for exponential growth and involves transient metal accumulation, J. Bacteriol. 194 (3) (2012) 686–701.
[26] S.C. Nunez, M.S. Ribeiro, A.S. Garcez, W. Miyakawa, Assessment of photodynamic damage on *Escherichia coli* via atomic force microscopy, Biophotonics: Photonic Solutions For Better Health Care II 7715 (2010) 1–8.
[27] M.J. Davies, Singlet oxygen-mediated damage to proteins and its consequences, Biochem. Biophys. Res. Commun. 305 (1) (2003) 761–770.
[28] P.S. Stewart, M.J. Franklin, Physiological heterogeinity in biofilms, Nat. Rev. Microbiol. 6 (3) (2008) 199–210.
[29] T.F. Mah, G.A. O'Toole, Mechanisms of biofilm resistance to antimicrobial agents, Trends Microbiol. 9 (1) (2001) 34–39.
[30] J.G. de Nobel, F.M. Klis, J. Priem, T. Munnik, H. van den Ende, The glucanase-soluble mannoproteins limit cell wall porosity in *Saccharomyces cerevisiae*, Yeast 6 (6) (1990) 491–499.
[31] F.M. Klis, P. Mol, K. Hellingwerf, S. Brul, Dynamics of cell wall structure in *Saccharomyces cerevisiae*, FEMS Microbiol. Rev. 26 (3) (2002) 239–256.
[32] M.J. Farrell, S.E. Finkel, The growth advantage in stationary-phase phenotype conferred by rpoS mutations is dependent on the pH and nutrient environment, J. Bacteriol. 185 (24) (2003) 7044–7052.
[33] S. Dantas Ada, A. Day, M. Ikeh, I. Kos, B. Achan, J. Quinn, Oxidative stress responses in the human fungal pathogen, *Candida albicans*, Biomol. Ther. 5 (1) (2015) 142–165.
[34] M.D. Ramírez-Quijas, R. Zazueta-Sandoval, A. Obregón-Herrera, E. López- Romero, M. Cuéllar-Cruz, Effect of oxidative stress on cell wall morphology in four pathogenic *Candida* species, Mycol. Prog. 14 (8) (2015).
[35] W.L. Chaffin, J.L. Lopez-Ribot, M. Casanova, D. Gozalbo, J.P. Martinez, Cell wall and secreted proteins of *Candida albicans*: identification, function, and expression, Microbiol. Mol. Biol. Rev. 62 (1) (1998) 130–180.
[36] D.W. Lowman, D.A. Ferguson, D.L. Williams, et al., Carbohydr. Res. 338 (14) (2003) 1491–1496.
[37] F.M. Klis, A. Boorsma, P.W. De Groot, Cell wall construction in *Saccharomyces cerevisiae*, Yeast 23 (3) (2006) 185–202.
[38] D. Alsteens, V. Dupres, K. Mc Evoy, L. Wilding, H.J. Gruber, Y.F. Dufrêne, Structure, cell wall elasticity and polysaccharide properties of living yeast microbial cells, as probed by AFM, Nanotechnology 19 (38) (2008) 384005.
[39] E. Dague, R. Bitar, H. Ranchon, F. Durand, H.M. Yken, J.M. François, An atomic force microscopy analysis of yeast mutants defective in cell wall architecture, Yeast 27 (8) (2010) 673–684.
[40] C. Formosa, M. Schiavoni, H. Martin-Yken, J.M. François, R.E. Duval, E. Dague, Nanoscale effects of caspofungin against two yeast species, *Saccharomyces cerevisiae* and *Candida albicans*, Antimicrob. Agents Chemother. 57 (8) (2013) 3498–3506.
[41] E. Canetta, G.M. Walker, A.K. Adya, Nanoscopic morphological changes in yeast cell surfaces caused by oxidative stress: an atomic force microscopic study, J. Microbiol. Biotechnol. 19 (6) (2009) 547–555.
[42] M. Schiavone, C. Formosa-Dague, C. Elsztein, M.A. Teste, H. Martin-Yken, M.A. de Morais Jr., E. Dague, J.M. François, Evidence for a role for the plasma membrane in the nanomechanical properties of the cell wall as revealed by an atomic force microscopy study of the response of saccharomyces cerevisiae to ethanol stress, Appl. Environ. Microbiol. 82 (15) (2016) 4789–4801.
[43] H.C. Flemminteg, J. Wingender, The biofilm matrix, Nat. Rev. Microbiol. 8 (9) (2010) 623–633.
[44] K.F. Mitchell, R. Zarnowski, D.R. Andes, The extracellular matrix of fungal biofilms, Adv. Exp. Med. Biol. 931 (2016) 21–35.
[45] M. Wainwright, K.B. Crossley, Methylene blue - a therapeutic dye for all seasons? J. Chemother. 14 (5) (2002) 431–443.
[46] P. Puja, S.M. Soumya, C.B. Subhash, S.K. Gopinatha, Exploring the interaction of phenothiazinium dyes methylene blue, new methylene blue, azure A and azure B with tRNAPhe: spectroscopic, thermodynamic, voltammetric and molecular modeling approach, Phys. Chem. Chem. Phys. 19 (9) (2017) 6636–6653.
[47] C.S. Oliveira, R. Turchiello, A.J. Kowaltowski, G.L. Indig, M.S. Baptista, Major determinants of photoinduced cell death: subcellular localization versus photosensitization efficiency, Free Radic. Biol. Med. 51 (4) (2011) 824–833.
[48] R.F. Donnelly, P.A. McCarron, M.M. Tunney, Antifungal photodynamic therapy, Microbiol. Res. 163 (2008) 1–12.